Influence of Angular Momentum on the Decay of the Ni^{60} Compound Nucleus*

J. BENVENISTE†
Aerospace Corporation, San Bernardino, Calfiornia 92402

AND

G. MERKEL
Office of Naval Research, Washington, D. C. 22311

AND

A. MITCHELL
Lawrence Radiation Laboratory, University of California, Livermore, California 94551

(Received 4 April 1968)

In an experiment designed to study the effect of angular momentum on compound-nucleus reactions, the Ni^{60} compound nucleus has been produced at the same excitation energy by bombarding two different target nuclei: Fe^{56}, with 20.7-MeV α particles, and Co^{59}, with 16.3-MeV protons. When α-particle and proton emission spectra from the Ni^{60} compound nucleus were separately measured at 10° intervals, the angular distributions were found to be generally symmetric about 90°. The α-particle-induced reactions, however, showed more compound-nucleus anisotropy than the proton-induced reactions. The experimental cross sections are compared with the predictions of the semiclassical compound-nucleus theory of Ericson and Strutinski.

INTRODUCTION

THE assumption of statistical randomness for compound-nucleus reactions in the continuum leads to a simplification in the interpretation of highly excited nuclei. In the work described in this paper we have attempted to study the effect of angular momentum on nuclear reactions that proceed by the statistically random compound-nucleus mechanism. This required the selection of target nuclei for which the experimental reaction mechanism would be principally compound-nucleus with a minimum contribution from less random direct mechanisms. Medium-weight elements were selected so that the level densities of the compound and residual nuclei would be sufficiently high that the statistical assumption would be valid while, at the same time, the Coulomb barrier would not be so high as to preclude the emission of the low-energy particles which make up such a large fraction of the compound-nucleus cross section.

Two sets of cross sections were measured by producing the Ni^{60} compound nucleus with an excitation energy of 24.6 MeV in two different ways: (1) 99.9%-enriched Fe^{56} target was bombarded with 20.7-MeV α particles and the resulting $Fe^{56}(\alpha,\alpha')$ and $Fe^{56}(\alpha,p)$ cross sections were measured. (2) A Co^{59} target was bombarded with 16.3-MeV protons and the resulting $Co^{59}(p,\alpha)$ and $Co^{59}(p,p')$ cross sections were measured. The essential difference between the α-particle- and proton-induced reactions is that, while both reactions produce the Ni^{60} compound nucleus at the same excitation energy, α-particle bombardment can produce a Ni^{60} compound nucleus with over twice the angular momentum of the Ni^{60} compound nucleus produced by proton bombardment.

In the early development of the statistical theory, Weisskopf[1] tacitly assumed a spin distribution in residual nuclei proportional to $2J+1$. This theory, based on the $2J+1$ assumption, leads to an isotropic angular distribution for emitted particles. Another result of the $2J+1$ assumption is that the shape of excitation-function curves involving the same compound nucleus is not a property of the bombarding particle. Ghoshal[2] showed that the shape of compound-nucleus excitation functions was not significantly influenced by the angular momentum of the bombarding particle.

Using a distribution of nuclear spins based on the assumption that the nucleus behaves as a rigid rotor, Ericson and Strutinski[3] obtained a more complicated, though more realistic, expression for nuclear reactions that proceed in a statistically random manner. These authors pictured the excited compound nucleus as a rigid rotor with moment of inertia I_{rig}. The rotational energy, therefore, is given by $\frac{1}{2}I_{\text{rig}}\omega^2=\hbar^2J^2/2I_{\text{rig}}$ in terms of the nuclear angular momentum J. Consequently, of the total excitation energy E, only the part $E-\hbar^2J^2/2I_{\text{rig}}$ is available for intrinsic excitation. If $\rho(E)$ is the level density of a nonrotating nucleus of excitation energy E, the model states that the level density of a system with excitation energy E and angular momentum J is given by

$$\rho(E-\hbar^2J^2/2I_{\text{rig}}) \propto \rho(E)\exp(-\hbar^2J^2/2I_{\text{rig}}T), \quad (1)$$

* The experimental portion of this work was performed when the authors were staff members of the University of California Lawrence Radiation Laboratory at Livermore, Calif.

† Present address: The Physics International Company, San Leandro, Calif.

[1] V. F. Weisskopf, Phys. Rev. **52**, 295 (1937).
[2] S. N. Ghoshal, Phys. Rev. **80**, 939 (1950).
[3] T. Ericson and V. Strutinski, Nucl. Phys. **13**, 382 (1958).

where T is the nuclear temperature. The theory based on the rigid-rotor spin distribution leads to angular distributions of evaporated particles that are symmetric around 90° but not necessarily isotropic. In general, the larger the maximum possible angular momentum introduced into a compound nucleus by the incident particle, the greater the anisotropy of the evaporated angular distributions.

EXPERIMENTAL ARRANGEMENT

The experimental equipment and procedures have been described in detail elsewhere.[4] The 99.9%-enriched Fe^{56} target foil and the Co^{59} target foil were approximately 1 mg/cm² in thickness. Great care was taken to construct a very thin dE/dx counter so that the α-particle spectra could be measured to energies appreciably below the Coulomb barrier. The lowest α-particle energy that could be measured with the detection system was about 2 MeV in the laboratory coordinate system.

It was difficult to prevent the target foils from being contaminated with organic compounds containing hydrogen, carbon, and oxygen. Therefore, in order to detect and properly compensate for their presence, a Mylar and a poyethylene target foil were mounted in the target holder. The peaks characteristic of elastic and inelastic α-particle or proton scattering from carbon, oxygen, and hydrogen were observed at each scattering angle after every Fe^{56} and Co^{59} bombardment. These observations yielded a quantitative measure of the impurity corrections which had to be made when some

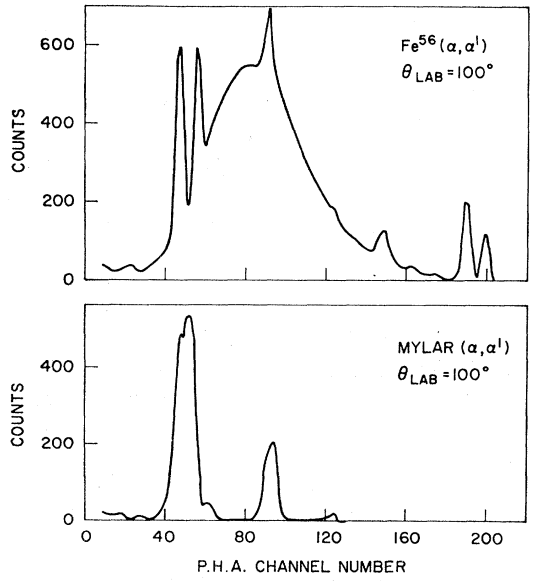

FIG. 1. Uncorrected α-particle spectra obtained by bombarding Mylar and Fe^{56} foils with 20.7-MeV α particles.

[4] J. Benveniste, G. Merkel, and A. Mitchell, Phys. Rev. 141, 980 (1965).

feature of the $Fe^{56}(\alpha,\alpha')$, $Fe^{56}(\alpha,p)$, $Co^{59}(p,\alpha)$ or $Co^{59}(p,p')$ overlaid an impurity peak.

A typical Mylar spectrum with the corresponding $Fe^{56}(\alpha,\alpha')$ spectrum is shown in Fig. 1. The treatment and reduction of the data are the same as described in Ref. 4.

EXPERIMENTAL RESULTS

Three types of comparisons of the α-particle and proton distributions emitted from the Ni^{60} compound nucleus, excited to 24.6 MeV, are shown in Figs. 2–5: (1) angular distributions produced with different projectiles, (2) energy spectra at different angles produced with the same projectile, and (3) energy spectra at the same angle produced with different projectiles.

Typical angular distributions are compared in Figs. 2(a) and 2(b). In Fig. 2(a) the $Fe^{56}(\alpha,p)Co^{59}$ and $Co^{59}(p,p')Co^{59}$ angular distributions are compared for 3.3-MeV protons. The anisotropy of the α-particle-induced reaction is much greater than that of the proton-induced reaction. The symmetric curved lines shown in Fig. 2(a) have been drawn only to show divergence from symmetry around 90°; they have not been calculated with the statistical theory. The experimental $Fe^{56}(\alpha,p)$ curve is symmetric around 90°, as is predicted by the compound-nucleus theory; however, the forward peaking evidenced by the (p,p') angular distribution is qualitatively consistent with a noncompound-nucleus contribution in the forward direction.

In Fig. 2(b) the $Fe^{56}(\alpha,\alpha')Fe^{56*}$ angular distribution of inelastically scattered 9.6-MeV α particles is compared to the 9.6-MeV α-particle angular distribution from the $Co^{59}(p,\alpha)Fe^{56}$ reaction. In this case, the symmetric curves have been calculated with the semiclassical theory of Ericson and Strutinski. These calculations will be discussed in the next section. Again, the α-particle-induced angular distribution is quite symmetric about 90°, while the proton-induced angular distribution indicates the presence of a nonstatistical direct-interaction reaction mechanism by peaking in the forward direction.

The experimental $Co^{59}(p,p')Co^{59}$ proton energy spectrum obtained at 90° is compared with the spectrum obtained at 160° in Fig. 3(a). The shapes of the proton spectra are generally consistent with a statistical theory evaporation spectrum except that, in the region of the highest proton energies, there is structure corresponding to the elastic peak and to some of the low-lying discrete nuclear energy levels near the elastic peak. As can be seen in Fig. 3(a), the experimental 160° evaporation spectrum has a maximum with a slightly larger cross-section value than the 90° spectrum.

The experimental $Co^{59}(p,\alpha)Fe^{56}$ evaporation spectra obtained at 90° and 160° are compared in Fig. 3(b). Again, the shapes of the spectra are qualitatively consistent with the predictions of the statistical theory. As in the case of the proton evaporation spectra, the 160°

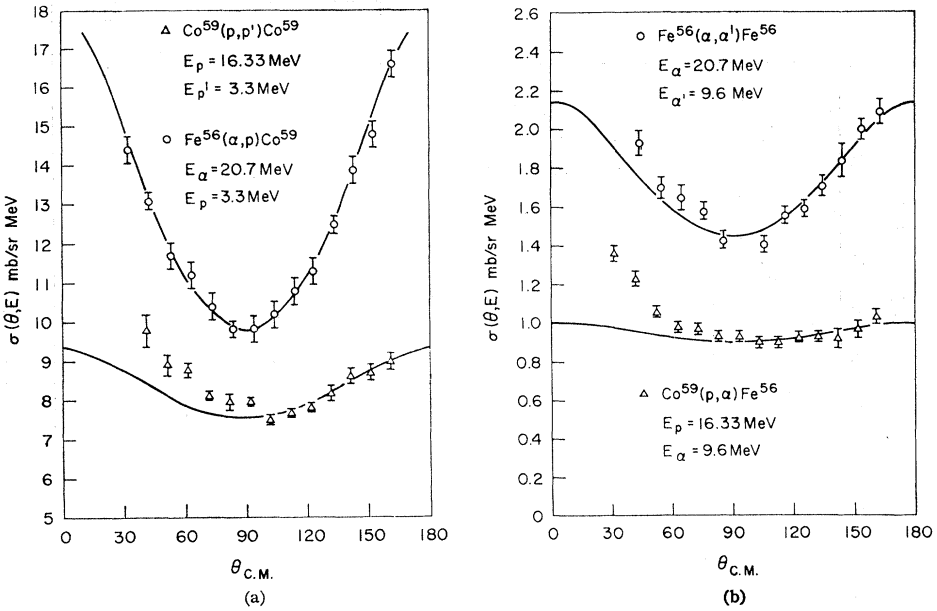

FIG. 2. (a) Comparison of $Fe^{56}(\alpha,p)Co^{59}$ and $Co^{59}(p,p')Co^{59}$ angular distributions. (b) Comparison of $Fe^{56}(\alpha,\alpha')Fe^{56}$ and $Co^{59}(p,\alpha)Fe^{56}$ angular distributions.

spectrum has a maximum with a slightly higher cross-section value than the 90° spectrum.

The $Fe^{56}(\alpha,p)Co^{59}$ evaporation energy spectra at 90° and 160° are compared in Fig. 4(a). The 160° proton evaporation spectrum of these α-induced reactions has a significantly larger maximum value than the 90° evaporation spectrum.

The $Fe^{56}(\alpha,\alpha')$ evaporation spectra at 80° and 160° are compared in Fig. 4(b). The 80° laboratory spectrum was chosen because it is closer to the 90° center-of-mass

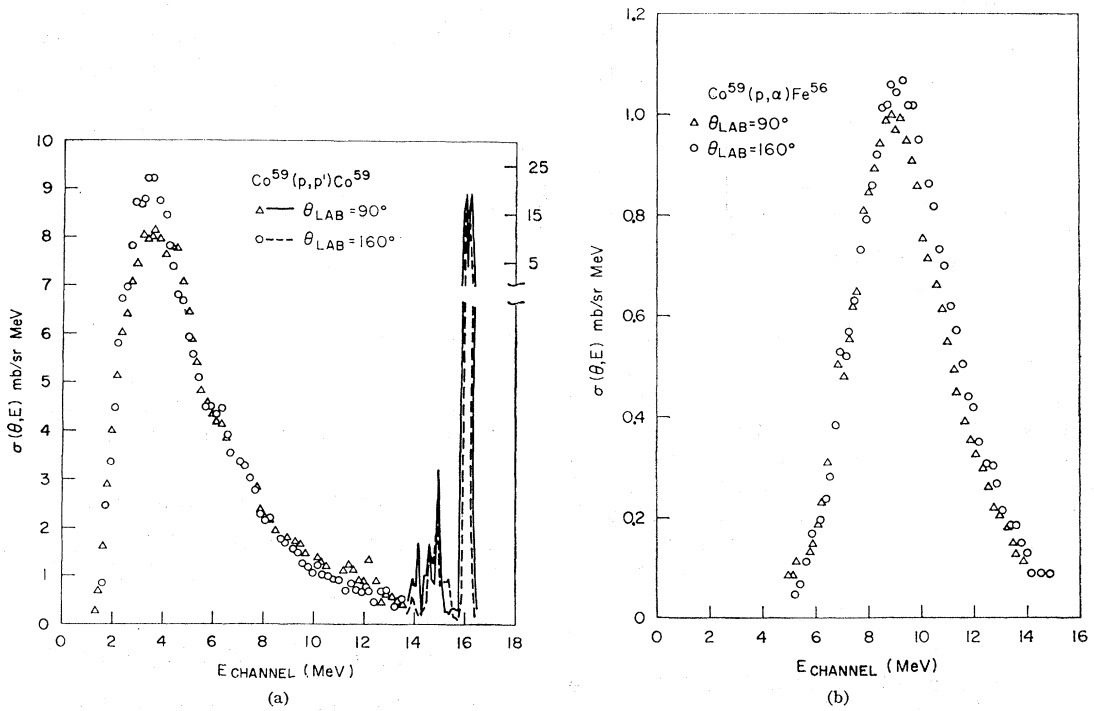

FIG. 3. (a) Comparison of $Co^{59}(p,p')Co^{59}$ energy distributions at laboratory angles of 90° and 160°. The incident proton energy is 16.3 MeV. (b) Comparison of $Co^{59}(p,\alpha)Fe^{56}$ energy distributions at laboratory angles of 90° and 160°. The incident proton energy is 16.3 MeV.

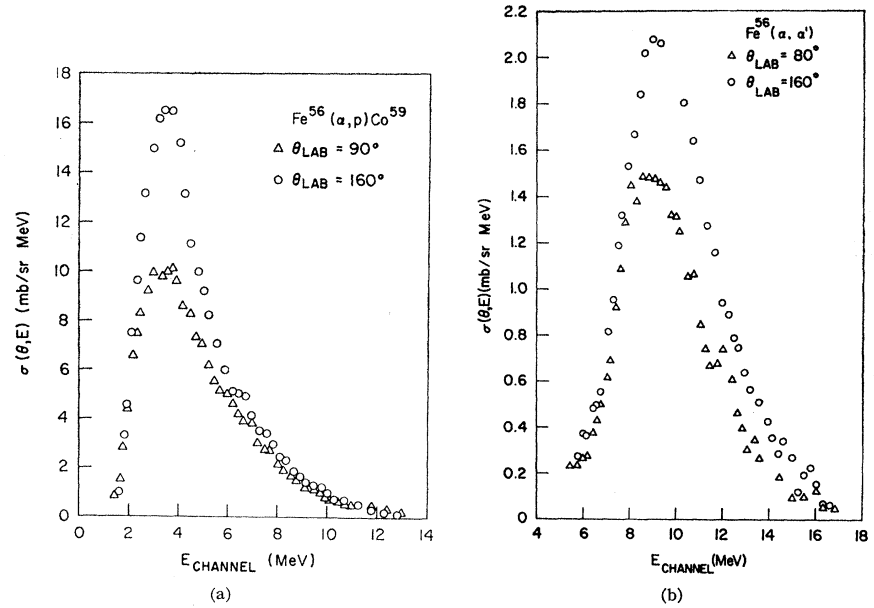

FIG. 4. (a) Comparison of $Fe^{56}(\alpha,p)Co^{59}$ energy distributions at laboratory angles of 90° and 160°. The incident α-particle energy is 20.7 MeV. (b) Comparison of $Fe^{56}(\alpha,\alpha')$ energy distributions at laboratory angles of 80° and 160°. The 80° laboratory angle is close to 90° in the center-of-mass system. The incident α-particle energy is 20.7 MeV.

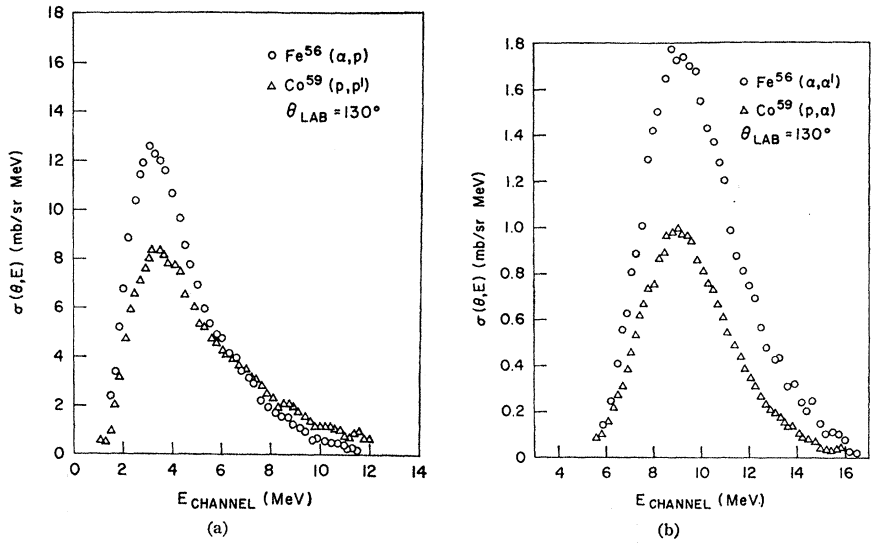

FIG. 5. (a) Comparison of $Fe^{56}(\alpha,p)$ and $Co^{59}(p,p')$ energy distributions at the laboratory angle of 130°. Both energy distributions correspond to a Ni^{60} compound nucleus excited to 24.6 MeV. (b) Comparison of $Fe^{56}(\alpha,\alpha')$ and $Co^{59}(p,\alpha)$ energy distributions at the laboratory angle of 130°. Both energy distributions correspond to a Ni^{60} compound nucleus excited to 24.6 MeV.

spectrum than the 90° laboratory spectrum. Again, the maximum cross-section value of the 160° α-particle evaporation spectrum is appreciably greater than the maximum value of the 80° evaporation spectrum.

Finally, evaporation spectra at the same laboratory angle from the Ni^{60} compound nucleus produced with different projectiles are shown in Figs. 5(a) and 5(b). Figure 5(a) shows a comparison between the experimental $Fe^{56}(\alpha,p)$ and $Co^{59}(p,p')$ evaporation cross sections at 130°, while Fig. 5(b) shows a comparison of experimental $Fe^{56}(\alpha,\alpha')$ and $Co^{59}(p,\alpha)$ evaporation cross sections, again at 130°.

The experimental results shown in Figs. 2–5 can be summarized as follows: (1) The compound-nucleus anisotropy of the α-particle-induced reactions is appreciably greater than that of proton-induced reactions; and (2) the deviation from symmetry around 90° due to the presence of nonrandom direct mechanisms is greater in the case of the proton-induced reactions than in the case of the α-particle-induced reactions.

THEORETICAL DISCUSSION

Ericson and Strutinski assumed that the distribution of states of the nucleus ν with spin J and excitation energy E_ν^* is given by

$$\rho(E_\nu^*,J)=(2J+1)\rho(E_\nu^*)\exp(-J^2/\sigma_\nu^2) \qquad (2)$$

and solved the compound-nucleus problem considering the restrictions imposed by the conservation of angular momentum. The differential cross section for the emis-

sion of a particle E_ν in the direction $\mathbf{n}$ is given by

$$\sigma(\mathbf{n},E_\nu)=\pi\lambda\!\!\!^{-}_i{}^2\int_0^\infty 2IT_I{}^{(i)}dI\frac{g_\nu\rho_\nu(E_\nu{}^*,0)\int_0^\infty 2lT_l{}^{(\nu)}(E_\nu)e^{-(I^2+l^2)/2\sigma_\nu{}^2}j_0(iIl/\sigma_\nu{}^2)W_{Il}(\mathbf{n},E_\nu)dl}{\sum_{\nu'}g_{\nu'}\int_0^\infty dE_{\nu'}\rho_{\nu'}(E_{\nu'}{}^*,0)\int_0^\infty 2lT_l{}^{(\nu')}(E_{\nu'})e^{-(I^2+l^2)/2\sigma_{\nu'}{}^2}j_0(Il/\sigma_{\nu'}{}^2)dl}, \tag{3}$$

where

$$W_{Il}(\mathbf{n},E_\nu)=\frac{1}{4\pi}\frac{\sum_k(-)^k(4k+1)[(2k)!/(2^k k!)^2]^2 j_{2k}(iIl/\sigma_\nu{}^2)P_{2k}(\cos\phi)}{j_0(iIl/\sigma_\nu{}^2)}, \tag{4}$$

and where $\lambda\!\!\!^{-}_i$ is the wavelength of the incident particle, θ is the scattering angle, j_{2k} is the spherical Bessel function of order $2k$, $T_I{}^i(I)$ is the transmission coefficient for the formation of a compound nucleus of angular momentum I by an incident particle, $T_l{}^\nu(E_\nu)$ is the transmission coefficient for a particle emitted with angular momentum l and energy E_ν[5], and g_ν is the statistical weight factor of the emitted particle due to its spin.

A derivation of the spin dependence of the level density may be obtained by considering a random coupling of the angular momenta of ν excited nucleons with mean-square magnetic quantum number $\langle m^2\rangle$. A comparison of the resulting expression with the rigid-rotor model discussed in the introduction yields the relation[6]

$$\sigma^2=\nu\langle m^2\rangle=I_{\text{rig}}T/\hbar^2. \tag{5}$$

Nuclear level densities have been discussed by many authors.[6–8] One explicit form of Eq. (2) is

$$\rho(E_\nu{}^*,J)=C_1(2J+1)(E_\nu{}^*-\Delta)^{-2}\exp[2\{a(E_\nu{}^*-\Delta)^2\}^{1/2}]\times\exp(-J^2/\sigma_\nu{}^2), \tag{6}$$

where, for a specific nucleus, C_1 remains a constant, a is the nuclear level density parameter, Δ is the pairing-energy correction, and σ^2 is the spin-cutoff parameter referred to in Eq. (5). The parameter a is related to the average nucleon level spacing δ at the Fermi level:

$$a=(\pi^2/6)(1/\delta). \tag{7}$$

[5] The values of $T_1(E_\nu)$ for protons used in the calculations in this paper are those tabulated by G. S. Mani, M. A. Melkanoff, and I. Iori, in Centre d'Etudes Nucléaires de Saclay Report No. 2379, 1963 (unpublished). The values of $T_1(E_\nu)$ for α particles are obtained from J. R. Huizenga and G. J. Igo, in Argonne National Laboratory Report No. ANL-6373, 1961 (unpublished). The values of $T_1(E_\nu)$ for neutrons are calculated with the Bjorkland-Fernbach Loki program with the parameters given by F. E. Bjorkland and S. Fernbach in Phys. Rev. **109**, 1295 (1958), except that the imaginary value of the optical-model potential is not allowed to decrease below 10 MeV. The reason for not using the smaller ground-state imaginary potentials at small values of E_ν is that the $T_1(E_\nu)$ in Eq. (3) correspond to excited residual nuclei. When a nucleus is excited, more phase space becomes available to scattered nucleons, the Pauli exculsion principle plays a less significant role, and the nucleus is expected to become less transparent.

[6] T. Ericson, Advan. Phys. **9**, 425 (1960).

[7] A. A. Ross, Phys. Rev. **108**, 720 (1957).

[8] D. Bodansky, Ann. Rev. Nucl. Sci. **12**, 79 (1962).

The nuclear temperature in Eq. (5) is given by

$$T=[(a-2)/(E_\nu-\Delta)]^{-1/2} \tag{8}$$

and the number of nucleons ν being coupled to produce the total angular momentum is given by $\nu=T/\delta$.

If nuclear shell effects are neglected, the nucleon level density parameter is usually assumed to be related to the nucleon mass number A by an expansion of the form $a=\text{const}\times A$; e.g., $a=A/10$. Newton[9] and Lang[10] have made semiempirical estimates of the influence of shell structure of a and σ^2. According to Newton,

$$a=0.0619(\bar{j}_n+\bar{j}_p+1)A^{2/3}, \tag{9}$$

where $\bar{j}_n$ and $\bar{j}_p$ are the means of j values for neutrons and protons, respectively, in the vicinity of the Fermi level being considered. Newton has tabluated values of $\bar{j}_n$ and $\bar{j}_p$ for all nuclei.

Equation (6) has a singularity when $E-\Delta=0$. This unphysical situation arises because of a number of simplifying assumptions made in the derivation of (6); e.g., a continuous distribution of nucleon states at the Fermi level is assumed so that integrations may be substituted for summations. Bloch[11] has obtained a more rigorous derivation of the nuclear level density, in which he does not substitute integrations for summations and which does not have a singularity near zero excitation energy. Unfortunately, Bloch's level-density equation is very complex and is not in a convenient closed form.

The singularity at $E-\Delta=0$ may be avoided in a somewhat artificial manner suggested by Durham and Halbert[12] and also by Bowsher[13]: Equation (6) is used only for $E-\Delta>16/a$; for the region $E-\Delta\leq 16/a$, one uses

$$\rho(E,J)=Ce^{-(E-\Delta)/T}e^{-I(I+1)\hbar^2/TI_{\text{rig}}}, \tag{10}$$

where $T=8/a$. The value of T used in Eq. (5) for the region $E-\Delta>16/a$ is given by Eq. (8). Equations (6) and (10) have the same value and the same slope at $E-\Delta=16/a$.

[9] T. D. Newton, Can. J. Phys. **34**, 804 (1956).

[10] D. W. Lang, Nucl. Phys. **26**, 434 (1961).

[11] C. Bloch, Phys. Rev. **93**, 1094 (1954).

[12] F. E. Durham and M. L. Halbert, Phys. Rev. **137**, B859 (1965).

[13] H. F. Bowsher, Bull. Am. Phys. Soc. **9**, 74 (1964); Oak Ridge National Laboratory Report No. ORNL-TM-971, 1964 (unpublished).

The value of the pairing energy Δ can be obtained from a recipe given by Newton[9]:

$$\Delta=0.82(4-A/100)\ \text{MeV}. \tag{11}$$

The simplest theoretical value of the spin-cutoff parameter is based on the rigid-rotor assumption $\sigma^2=I_{\text{rig}}T$. This assumption neglects shell effects. We could also use the extreme shell model and obtain

$$\sigma^2=\nu\langle m\rangle^2 =\nu\frac{\langle j_n(j_n+1)(2j_n+1)+j_p(j_p+1)(2j_p+1)\rangle_{\text{av}}}{(2\bar{j}_n+2\bar{j}_p+2)},$$

where the values of j_n and j_p are the same as those that appear in Eq. (9) and ν is defined as in Eq. (5). However, as Newton[9] has indicated, the mixing of nuclear states has a much greater effect on $\langle m\rangle^2$ than on the average nucleon level spacing δ. The value of $\langle m\rangle^2$ is especially sensitive to assumptions about states of high spin. Newton, therefore, adopted the easier course and used the rigid-rotor prediction for $\langle m\rangle^2$ given by Eq. (5).

If a nuclear reaction proceeds via the statistically random compound-nucleus mechanism and if the distribution of nuclear levels and spins of the various residual nuclei are known, the statistical theory can be used to calculate both the magntiude and the shape of the various angular and energy distributions. The task we have undertaken is to calculate the $Fe^{56}(\alpha,\alpha')Fe^{56*}$, $Fe^{56}(\alpha,p)Co^{59}$, $Co^{59}(p,p')Co^{59*}$, and $Co^{59}(p,\alpha)Fe^{56}$ cross sections using the Ericson-Strutinski formulation of compound-nucleus reactions. The three principal decay modes of the Ni^{60} compound nucleus are $Ni^{60}\rightarrow Ni^{59}+n$, $Ni^{60}\rightarrow Co^{59}+p$, and $Ni^{60}\rightarrow Fe^{56}+\alpha$. Thus, one seeks a consistent set of nuclear level density parameters for Eq. (6) (i.e., values of a, σ^2, and Δ for Ni^{59}, Co^{59}, and Fe^{56}, respectively) which yield cross sections [calculated with Eq. (3)] that match the experimental cross sections.

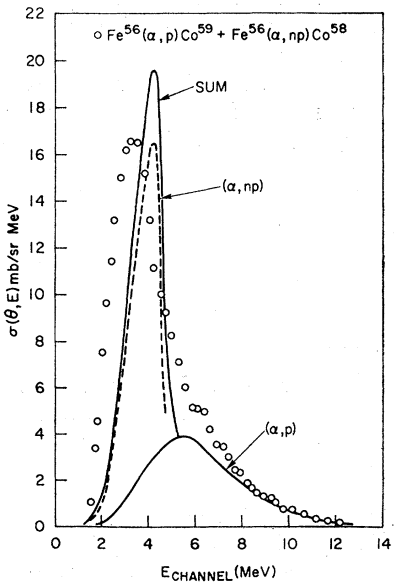

FIG. 6. Conventional compound-nucleus calculation of the $Fe^{56}(\alpha,p)Co^{59}+Fe^{56}(\alpha,np)Co^{58}$ cross sections. The points correspond to the $Fe^{56}(\alpha,p)$ cross sections at 160°.

A complication worthy of consideration in the interpretation of the experimental results is the emission of particles in cascade, for the excitation energy of the Ni^{60} compound nucleus (24.6 MeV) is high enough to allow multiple-particle emissions. As an estimate of the magnitude of the $Fe^{56}(\alpha,n\alpha)Fe^{55}$, $Fe^{56}(\alpha,p\alpha)Mn^{55}$, $Fe^{56}(\alpha,np)Co^{58}$, $Fe^{56}(\alpha,2p)Fe^{58}$, $Co^{59}(p,n\alpha)Fe^{55}$, $Co^{59}(p,p\alpha)Mn^{55}$, $Co^{59}(p,np)Co^{58}$, and $Co^{59}(p,2p)Fe^{58}$ reactions, we have employed the compound-nucleus theory as described in Blatt and Weisskopf[14,15] (based on the assumption that $\rho_J\propto 2J+1$).

Figure 6 shows the result of a conventional compound-nucleus calculation for the $Fe^{56}(\alpha,p)Co^{59}$ and $Fe^{56}(\alpha,np)Co^{58}$ cross sections. In a calculation based on the assumption that $\rho_J\propto 2J+1$; the mode of formation of the compound nucleus (i.e., whether the Ni^{60} at an excitation energy of 24.6 MeV is produced by $p+Co^{59}$ or $\alpha+Fe^{56}$) does not effect the calculated evaporation spectra from the Ni^{60} compound nucleus. The calculations shown in Fig. 6, therefore, also apply to the $Co^{59}(p,p')Co^{59}$ and $Co^{59}(p,np)Co^{58}$ compound-nucleus cross sections. The conventional calculation, although an approximation, indicates that contributions from the $Fe^{56}(\alpha,np)$ and $Co^{59}(p,np)$ reactions should be considered in the interpretation of the $Fe^{56}(\alpha,p)$ and $Co^{59}(p,p')$ experimental evaporation spectra.

A similar conventional calculation indicates that the probability of emission of an α particle after proton or neutron emission is negligible. If the results of a conventional calculation can be used as a guide, it is reasonable to calculate the $Fe^{56}(\alpha,\alpha')$ and $Co^{59}(p,\alpha)$ cross sections with Eq. (3) without considering cascade emissions

The results of these conventional calculations may be intuitively understood in terms of the large α-particle Coulomb barrier. After a neutron or proton has been emitted from the 24.6-MeV Ni^{60} compound nucleus, another proton may be emitted, but the α-particle Coulomb barrier prevents the emission of an α particle.

Even though Eq. (3) is not applicable to the entire range of $Co^{59}(p,p')$ and $Fe^{56}(\alpha,p)$ experimental proton energy spectra, Eq. (3) should describe those portions of the experimental energy spectra for which multiple-particle emissions are excluded by binding-energy and Coulomb-barrier considerations. That is to say, the

[14] J. Blatt and V. F. Weisskopf, *Theoretical Nuclear Physics* (John Wiley & Sons, Inc., New York, 1952), p. 340.

[15] The nuclear level density expression used to obtain the calculated curves shown in Fig. 6 is

$$\rho(E_\nu^*)=C_1(E_\nu^*-\Delta)^{-2}\exp[2\{a(E_\nu^*-\Delta)^2\}^{1/2}],$$

where E_ν^*, Δ, and a are the same as in Eq. (6). The nuclear level density parameter was assumed to be given by $a=A/10$. The sources of the inverse capture cross sections are described in Ref. 5.

proton emission cross sections calculated with Eq. (3) should approach the experimental curves for proton emission energies greater than about 6 MeV.

Assuming a level density of the form given by Eq. (2), Douglas and MacDonald[16] have derived an expression for the emission of two particles in cascade in which the many possible combinations of angular momenta of the residual nuclei and emitted particles are considered. However, the amount of computer time necessary for such a calculation is beyond our means. The problem is compounded because it is necessary to search for six additional sets of level density parameters for residual nuclei resulting from neutron, proton, or α-particle emission from the Ni^{59} or Co^{59} intermediate compound nuclei. We, therefore, have not attempted to interpret that portion of the proton emission spectra corresponding to (α,np), $(\alpha,2p)$, (p,np), and $(p,2p)$ reactions.

PROCEDURE FOR CHOOSING NUCLEAR LEVEL PARAMETERS

As discussed in the previous section, if the nuclear reactions proceed by the compound-nucleus mechanism, the $Fe^{56}(\alpha,\alpha')Fe^{56}$, $Co^{59}(p,\alpha)Fe^{56}$, $Fe^{56}(\alpha,p)Co^{59}$, and $Co^{59}(p,p')Co^{59}$ cross sections are calculable if the nuclear level densities of Fe^{56}, Co^{59}, and Ni^{59} are known. Therefore, we shall use Eqs. (3), (6), and (10) to describe and interpret our experimental data.

In order to avoid invoking a large number of parameters, the simplest assumption, that σ^2 behaves according to the rigid-rotor model, will be used. The pairing-energy correction will be calculated with Eq. (11). For odd-odd nuclei, $\Delta=0$; for odd-even nuclei, Δ is given by Eq. (11); and for even-even nuclei, Δ is twice the value given by Eq. (11). The task is then to find values of the nuclear level parameter a in Eqs. (6) and (8) for Fe^{56}, Ni^{59}, and Co^{59} which yield the most satisfactory agreement with our experimental results.

The $Fe^{56}(\alpha,\alpha')$ and $Co^{59}(p,\alpha)$ cross sections were calculated first because the simple calculations described in the previous section indicated that the probability of neutron or proton emission before α-particle emission is very small. In general, the magnitude of the anisotropy in the $Fe^{56}(\alpha,\alpha')$ and $Co^{59}(p,\alpha)$ differential cross sections was found to be most sensitive to the value of the spin-cutoff parameter σ^2 chosen for Fe^{56} (or to the value of I_{rig}) and relatively insensitive to the values of the nuclear parameter a. The rigid-rotor moment of inertia is $I_{\text{rig}}=\frac{2}{5}R_0A^{5/3}$, where $R_0=1.07$ F gave good agreement with the experimental α-particle angular distributions. On the other hand, the shapes of the $Fe^{56}(\alpha,\alpha')Fe^{56}$ and of the $Co^{59}(p,\alpha)Fe^{56}$ α-particle energy distributions were found to be very sensitive to the parameter a chosen for Fe^{56}. The absolute values of the α-particle energy and angular distributions may then be obtained by choosing values of the nuclear level parameter a for Co^{59} and Ni^{59}. Next, it is necessary that the value of the parameter a for Co^{59} produce proton energy spectra that agree with the shape of the experimental $Fe^{56}(\alpha,p)$ and $Co^{59}(p,p')$ spectra for proton

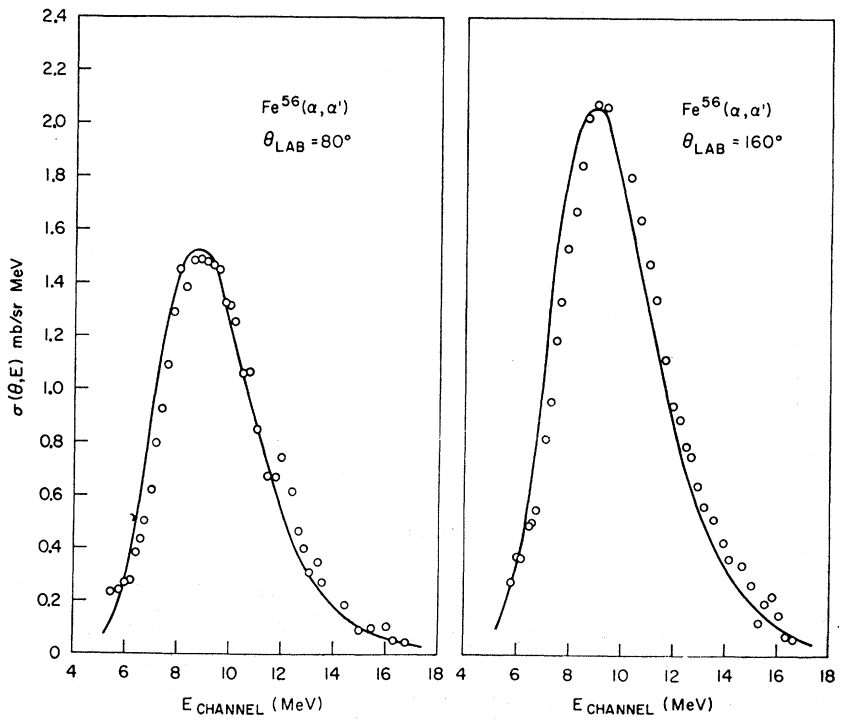

FIG. 7. Comparison of experimental $Fe^{56}(\alpha,\alpha')$ cross sections with cross sections calculated with Eq. (3). The values of the nuclear level density parameters used in the calculation are given in Table I.

[16] A. C. Douglas and N. MacDonald, Nucl. Phys. **13**, 382 (1959).

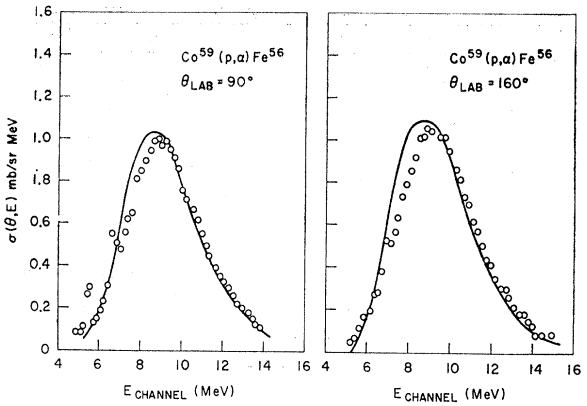

FIG. 8. Comparsion of experimental $Co^{59}(p,\alpha)$ cross sections with cross sections calculated using Eq. (3). The values of the nuclear level density parameters used in the calculation are given in Table I.

energies greater than approximately 6 MeV. Once the value of a for Co^{59} has been determined from the $Fe^{56}(\alpha,p)$ and $Co^{59}(p,p')$ energy spectra, one nuclear level parameter is left, namely, the value of a corresponding to Ni^{59}. The value of the parameter a for the Ni^{59} residual nucleus is chosen so that the absolute values of the calculated cross sections correspond to the experimental cross sections.[17] The final results are shown in Figs. 7 to 11. The values of the nuclear level parameters are shown in Table I. The fact that the values for a in Ni^{59} agreed to within 20% implies satisfactory agreement with the theory within the uncertainties introduced by calculations of the transmission coefficients, neglect of

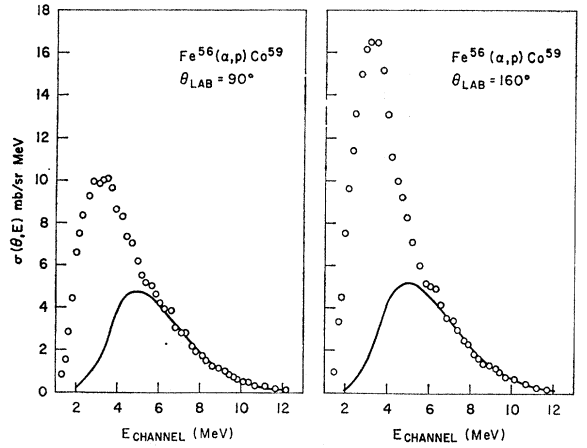

FIG. 9. Comparsion of experimental $Fe^{56}(\alpha,p)$ cross sections with $Fe^{56}(\alpha,p)Co^{59}$ cross sections calculated using Eq. (3). The values of the nuclear level density parameters used in the calculation are given in Table I. The difference between the calculated curves and the experimental curves in the region $E_{\text{channel}}<6$ MeV is due to contributions from the $Fe^{56}(\alpha,np)Co^{58}$ and the$Fe^{56}(\alpha,2p)$ Fe^{58} reactions.

[17] Typically, a 4% increase in the value of a for Ni^{59} results in approximately a 40% decrease in the absolute value of the calculated (α,α') cross section.

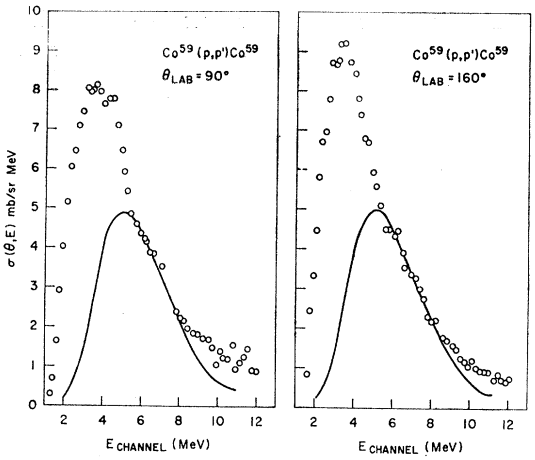

FIG. 10. Comparsion of experimental $Co^{59}(p,p')$ cross sections with $Co^{59}(p,p')Co^{59}$ reactions calculated with Eq. (3). The values of the nuclear level density parameters used in the calculation are given in Table I. The difference between the calculated curves and the experimental curves in the region $E_{\text{channel}}<6$ MeV is due to contributions from the $Co^{59}(p,np)Co^{59}$ and theCo^{59} $(p,2p)$ Fe^{58} reactions.

the spin of the target nucleus, and the assumption that the imaginary part of the optical potential yields the probability of formation of the compound nucleus.

CONCLUSIONS

In general, the qualitative behavior of the $Fe^{56}(\alpha,\alpha')$, $Fe^{56}(\alpha,p)$, $Co^{59}(p,\alpha)$, and $Co^{59}(p,p')$ reactions is consistent with the statistical theory of compound nuclei as applied to the continuum, except that there is a tendency for some forward peaking at scattering angles less than 80°. The behavior of the compound-nucleus angular distributions in the $p+Co^{59}$ and $\alpha+Fe^{56}$ reactions was found to be consistent with the predictions of the rigid-rotor model where the nuclear moment of inertia is calculated by $I_{\text{rig}}=\frac{2}{5}R_0^2A^{5/3}M$ (A is the nuclear mass number, M is the nucleon mass, and $R_0=1.07$ F).[18] In the Ni^{60} compound nucleus, excited to 24.6 MeV produced by the $p+Co^{59}$ and $\alpha+Fe^{56}$ reactions, we have found a definite angular momentum

TABLE I. Nuclear level density parameters in MeV^{-1} yielding best fit.

Reaction	Residual nuclei Fe^{56}	Co^{59}	Ni^{59}
$Fe^{56}(\alpha,\alpha')Fe^{56}$	5.50[a]	6.40	5.50
$Co^{59}(p,\alpha)Fe^{56}$	5.50	6.40	6.05
$Fe^{56}(\alpha,p)Co^{59}$	5.50	6.40	5.65
$Co^{59}(p,p')Co^{59}$	5.50	6.40	5.80

[a] The difference between this value and that derived in Ref. 4 (i.e., $a=7.0$ MeV^{-1}) may be due to differing assumptions on the I dependence of Γ_I, the total decay width. In the earlier paper, Γ_I was assumed to be constant whereas, in this paper, Γ_I was calculated explicitly.

[18] As in the case of the nuclear level density parameter a (Table I), the explanation of the difference between the value of R_0 reported here and the value reported in Ref. 4 lies in the explicit calculation of Γ_I.

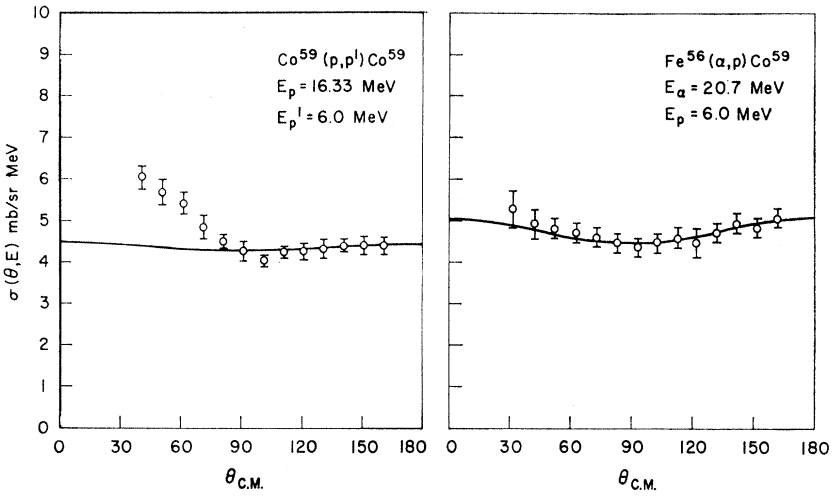

FIG. 11. Comparison of the experimental $Co^{59}(p,p')Co^{59}$ and $Fe^{56}(\alpha,p)Co^{59}$ angular distributions for protons emitted with an energy of 6 MeV. The curves have been calculated using Eq. (3) with the nuclear level density parameters given in Table I. The forward peaking of the experimental $Co^{59}(p,p')Co^{59}$ distribution is consistent with the presence of a noncompound-nucleus reaction mechanism. Note that the $Co^{59}(p,p')$ proton distribution shown in Fig. 2(a) is also peaked at forward angles.

effect. Specifically, the anisotropy of the α-induced reactions was much greater than that of the proton-induced reactions [e.g., Fig. 2(a)]. We attempted to calculate the set of four experimental cross sections with a consistent set of nuclear level density parameters and found that we could use the same parameters for Fe^{56} ($a=5.50$ MeV^{-1}) and Co^{59}($a=6.40$ MeV^{-1}) but had to allow the Ni^{59} nuclear level density parameter a to range from 5.50 MeV^{-1} to 6.05 MeV^{-1} (with an average value of 5.75 MeV^{-1}) in the four reactions studied. Using Newton's recipe, Eq. (9), we obtain for a the values 6.66 MeV^{-1} for Fe^{56}, 6.54 MeV^{-1} for Co^{59}, and 5.95 MeV^{-1} for Ni^{59}. In the light of the uncertainty in the values of the transmission coefficients, the expression used for the nuclear level density, and the fact that the calculations are semiclassical and do not consider the spin of the Co^{59} target nucleus, the quality of the agreement is remarkable.

A possible insight into the reasons for difference between the values of the nuclear level density parameters a derived from the experimental cross-section data and the values of a obtained with Newton's Eq. (9) may be obtained from a consideration of the assumptions and simplifications implicit in the derivation of the nuclear level density of Eq. (6). In the nuclear-mass region of deformed nuclei, the degeneracies of the nucleon levels of the extreme shell model are removed, and the averaging of nucleon level spacings to obtain an average value of the nucleon level spacing δ is reasonable. However, as Bloch[11] and Rosenzweig[19] have indicated, application of Eq. (6) in the region of a closed shell is open to criticism. One of the principal decay modes of the Ni^{60} compound nucleus is the neturon decay of Ni^{60} to the closed proton shell Ni^{59} nucleus. A more sophisticated calculation based on a level-density expression such as that described by Bloch might be an approach which resolves the discrepancy.

ACKNOWLEDGMENTS

The authors are especially indebted to Dr. M. Halbert for the use of his Fortran program for the calculation of compound-nucleus cross sections with the Ericson and Strutinski compound-nucleus cross-section expression, Eq. (3). The cooperation of Don Rawles and the Livermore cyclotron crew is greatly appreciated.

[19] N. Rosenzweig, Phys. Rev. **108**, 817 (1957).